Journal of the European Ceramic Society 20 (2000) 1159–1167

Mechanical and thermal shock properties of size graded MgO–PSZ refractory

Wen-Cheng J. Wei*, Yuh-Pring Lin

Institute of Materials Science and Engineering, National Taiwan University, Taipei, Taiwan 106, ROC

Received 17 February 1999; received in revised form 26 August 1999; accepted 12 September 1999

Abstract

The effects of the mixture of coarse powder with fine PSZ powder on the thermal-mechanical properties of 10 Mg–PSZ samples were studied. The size graded specimens were injection-molded using 3.5 m% MgO–ZrO_2 powders. The physical properties of the ZrO_2 samples and five thermal shock parameters were measured and calculated. These properties included density (ρ), porosity (p), the ratio of m/(t + c + m) phase, fracture toughness (K_{IC}), strength (σ_f), Young's modulus (E), shear modulus (G), Poisson's ratio (ν), and the thermal expansion (α) between ambient temperature to 1100°C. The toughness and thermal shock resistance of the PSZ are controlled by the states of porous microstructure which can be represented by a parameter (nominal largest tolerable length of defects) a_t. The PSZ samples show two types of thermal shock behavior differentiated by comparing the value of a_t to the characteristic length L_f of the defects in the sintered PSZ. The states of the defects, i.e. porosity, are the microstructural evidence to explain the relationship between the thermal shock properties.

Keywords: Mechanical properties; Refractories; Thermal properties; Thermal shock; ZrO_2

1. Introduction

Zirconia is a high temperature resistant material with excellent thermal insulation property currently used as a refractory,[1] which is especially resistant to the corrosion caused by basic slags in the continuously casting of molten steel. However, the thermal expansion of the material is very high among structural ceramics. Those unfavorable thermomechanical properties make zirconia materials very sensitive to thermal shock.

Bullard and Cheng[2] reported that a ZrO_2 nozzle with a smaller grain size was easily spalled during thermal shock and the catastrophic failure of the refractory parts limits the application for long-term service. They further reported that a zirconia refractory with controlled porosity and density, and a greater consistency in texture would perform better at high temperature.

For the past two decades, zirconia has greatly improved in toughness[3,4] and the strength is greatly controlled by the type and amount of monoclinic (m) phase in the zirconia materials (TZP and PSZ). The transformation toughening occurring at an ambient temperature has made zirconia useful in several stringent applications. However, the transformation toughening is not effective at high temperatures, nor occurs in the conditions of thermal cycling. Very few high temperature applications of zirconia have emphasized the merits of the toughening effects. Alternatively, destabilization of ZrO_2,[5,6] microstructural modifications[7,8] or grain size optimization[9] in other ceramic systems have proven to be capable of improving thermal shock properties.

One of the microstructural modifications was reported by Lutz et al.[7] on a series of ceramic composites with a duplex microstructure. The improvement of thermal shock properties can be retrieved from the crack deflection and branching using a reinforced second phase. The agglomerated ZrO_2 inclusions have strengthened the neighboring matrix and undergo transformation toughening so to adsorb fracture energy. Among the cases presented, the size and distribution of the second-reinforced zirconia inclusions are the primary properties of the composite.

In our previous work,[10] a series of zirconia with fine/coarse mixtures was prepared using an injection molding

* Corresponding author at: 1 Roosevelt Road, Sec. 4, Taipei, Taiwan 106, ROC. Tel.: +886-2-23632684; fax: +886-2-23634562.
E-mail address: wjwei@ccms.ntu.edu.tw (Wen-Cheng J. Wei).

0955-2219/00/$ - see front matter
PII: S0955-2219(99)00243-5

techniques. The zirconia samples with uniform microstructures were sintered in different conditions to achieve various porous and grain structures. The designed microstructures with unique features, combined coarse grains, pores, and cracks, are desirable for a fundamental study. The samples were prepared with a similar content of m-phase. It can differentiate the contributions of the structural factors from the phase transformation of the size-grading zirconia.

2. Experimental

2.1. Materials

Two zirconia powders and one MgO powder were used for the preparation of the partially stabilized zirconia (PSZ) mixture. One is the coarse powder (AQZ-100, Universal Abrasives, UK) with an angular shape and in an average particle size of 60 μm. The AQZ powder appeared as a PSZ has a magnesia and calcia contents of 3.66 and 0.3 mass%. The other is the fine powder (non-stabilized, EF-PREMIUM, Z-Tech Co., USA) in an average particle size of 1.0 μm, which appears as a spherical shape and mild agglomeration.

Five sets of the PSZ samples were formulated, F00–F100, containing the fine EF powder from 0 to 100 mass%. To keep the MgO content constant, 3.6 ± 0.1 mass%, in all formulations, an MgO powder was used which was prepared from the calcination of a hydrolyzed magnesium carbonate powder (City Gate International Co., Ltd., ROC).

2.2. Injection molding and sintering

The powders were mixed with a binder system and injection molded. The details concerning kneading of the feedstocks, injection molding, solvent and thermal debindings are described in the previous paper.[10] After injection-molding and debinding, the samples were sintered at the temperatures of 1450∼1750°C. The details of sintering conditions are shown in Table 1.

2.3. Characterization

The density of sintered samples was measured by Archimedes' method. The PSZ samples in different grinding and heat-treatment stages were tested using an X-ray diffractometer (XRD, PW1792, Philips Instrument, Netherlands). The amount of monoclinic phase in the as-sintered zirconia was determined following a quantitative XRD technique reported by Garvie et al.[11]

An ultrasonic instrument (DTM 12, Krautkramer-Branson Co., Ltd., Germany) was used for the measurement of elastic and shear moduli, and Poisson's ratio. The velocities of transverse and longitudinal waves of 5 MHz were measured to calculate the PSZ properties according to the ASTM standard (C1198-91).

The four-point bending test of ASTM C1161-90 was conducted for the measurement of the bending strength of PSZ samples. The single edge notched beam (SENB) method[12] was used for the measurement of the toughness of the zirconia test bars. Both tests were executed on an MTS universal testing machine (model 810, MTS Co., USA). Each data point was averaged from at least either 10 (σ_f measurement) or four (K_{IC}) measurements.

The thermal shock resistance of PSZ was evaluated by using the same PSZ test bars as used in the four-point bending test. The test bar was pre-heated to a specified temperature for 30 min, then quenched in distilled water (25°C). The quenched sample was dried and the retained strength of the PSZ was measured.

A scanning electron microscope (Mini-SEM, JEOL Co., Japan) was used to observe the polished and fracture

Table 1
The assigned symbol, sintering and physical properties of 10 Mg–PSZ specimens sintered in different conditions

Symbol[a]	Range of density (g/cm^3)	Sintering temperature and time	Bulk density (g/cm^3)	Total or closed porosity (%)	K_{IC} (MPa $m^{1/2}$)	σ_f (MPa)	E (GPa)	ν	$\alpha \times 10^{-6}$ (K^{-1})[b]	γ (Pa m) or (J/m^2)[c]
F100H	5.4	1700°C×4 h	5.36	6.5,6.5	5.40	441	213	0.25	13.7	64.2
F100M	5.0	1450°C×1 h	4.98	13.1,5.5	3.24	243	187	0.14	11.6	27.5
F75H	5.0	1700°C×4 h	4.97	13.3,5.8	2.71	248	199	0.18	13.8	17.8
F75M	4.6	1450°C×3 h	4.65	18.9,0.4	1.45	142	155	0.26	12.0	9.0
F50H	4.6	1700°C×4 h	4.56	22.2,0.7	4.40	133	161	0.19	14.1	57.9
F75L	4.3	1450°C×1 h	4.34	24.3,0.3	1.18	137	124	0.20	11.9	9.3
F50M	4.3	1550°C×1 h	4.22	27.0,0.5	2.58	53	131	0.19	12.4	24.5
F25	3.9	1700°C×4 h	3.93	32.1,0.0	1.39	67.9	83.6	0.22	12.9	11.0
F50L	3.7	1450°C×1 h	3.80	33.9,0.0	1.72	54.6	85.8	0.21	12.0	16.5
F00	3.7	1700°C×4 h	3.67	36.5,0.0	0.92	42.2	88.7	0.20	14.0	4.6

[a] H, relatively high density; M, medium density; L, relatively low density.
[b] α is calculated within 20∼1000°C.
[c] $\gamma = K_{IC}^2(1-\nu^2)/2E$.

surfaces of the PSZ at different stages. After polishing, the specimens were etched with 48% HF solution at 20°C for 4 min to reveal the grain boundaries.

3. Results

3.1. Density and crystalline phase

In order to distinguish the effects of coarse/fine powder ratio on the microstructure and on the physical properties of the PSZ, six ranges of the density (from 5.4 to 3.7 g/cm^3) and 10 PSZ samples are prepared, as shown in Table 1. The porosity of the PSZ ranges from 6.5 to 36%, being mostly open porosity. Only three exceptions, either F100H, F100M or F75H, had closed porosity of 6.0–5.5%. In addition, there is no open porosity in F100H. Most of the closed pores are in the sizes 4 to 16 μm located at the grain boundaries.

Because the surfaces of the sintered PSZ samples were not flat, surface machining by diamond wheel followed by heat-treatment was required. The m-phase of the PSZ was 5 ± 1% after sintering at 1650°C.But the m-phase of the F100 increases to 16% once they were ground by a diamond wheel, as shown in Fig. 1. However, the amount of m-phase would reduce to 6 or 13% when the ground samples were treated at 1400 or 1450°C for less than 1 h. Moreover, the quantity of m-phase would increase as the time of the heat treatment extended. Therefore, the samples for the following test would undergo surface grinding and heat-treatment at 1400°C for 2 h to ensure the m/(t + m + c) phase ratio of all PSZ remaining 20 ± 2%. No r-phase is found from the XRD patterns.

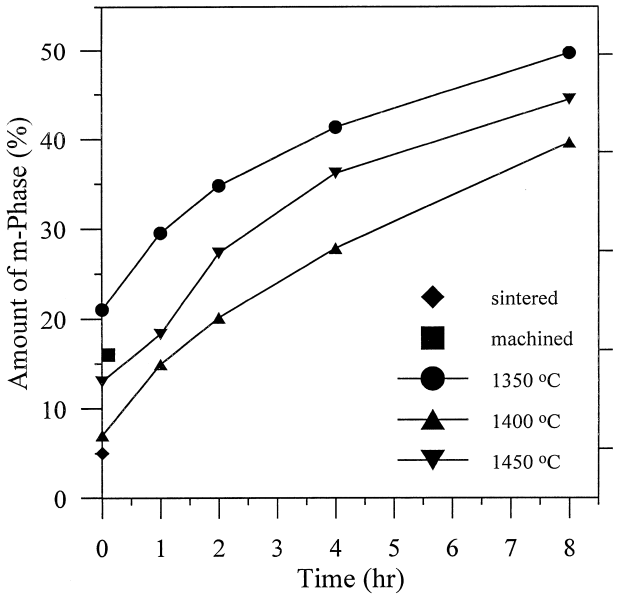

Fig. 1. The amount of m-phase of F100 PSZ sample either as-sintered, or followed diamond-wheel grinding, then heat-treated at 1350 to 1450°C plotted as a function of heat-treatment period.

3.2. Material properties of PSZ

The elastic modulus, shear modulus and Poisson's ratio of the PSZ as a function of porosity are reported in Fig. 2. The magnitude of the elastic modulus or shear modulus decreases as the porosity increases. Two properties of 10 PSZ are plotted and fitted by semi-empirical equations. They show

$$E = E_0 \exp(-AP) \text{ or } G = G_0 \exp(-BP) \quad (1)$$

where E_0 and G_0 are the elastic and shear moduli, respectively, of the PSZ with zero porosity, and A and B are constants. The values of E_0 and G_0 are estimated from Fig. 2 to be 296 GPa and 186 MPa, respectively. The elastic modulus of the best sample, F100H, (213 GPa) is lower than the calculated E_0, but close to the value (200 GPa) reported in the literature.[13] In contrast, the Poisson's ratio values, varied from 0.14 to 0.26, of these PSZ (Fig. 2) are rather scattered, especially for the samples with a higher density. But the values converge to 0.20 as the porosity of the PSZ is greater than 20%. The variation of the ratio is also possibly limited by the capability of the ultrasonic technique. Poisson's ratio data of PSZ is not available in literature to make a comparison.

The thermal expansion data of 10 PSZ are reported in Fig. 3, and the average CTE values are calculated in the range of $12.8 \pm 1.2 \times 10^{-6}$/K. The expansion and shrinkage behaviors of six Mg-stabilized PSZ did not show the t/m transformation above room temperature. It means that the Martensitic transformation (M_s) temperature can be measured only below room temperature. However,

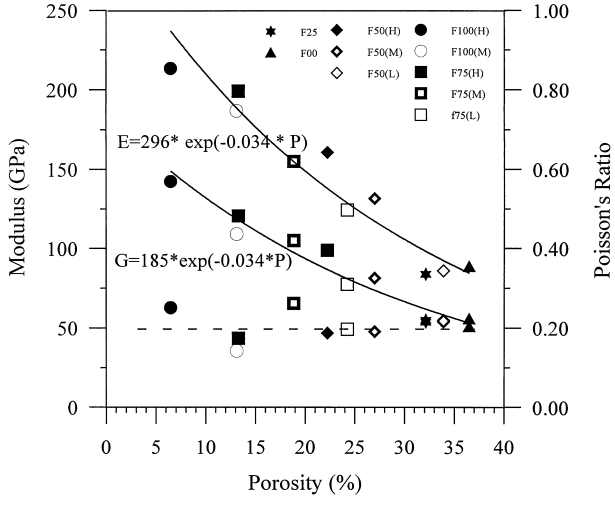

Fig. 2. Elastic modulus (E), shear modulus (G) and Poisson's ratio (v) of the PSZ plotted as a function of porosity.

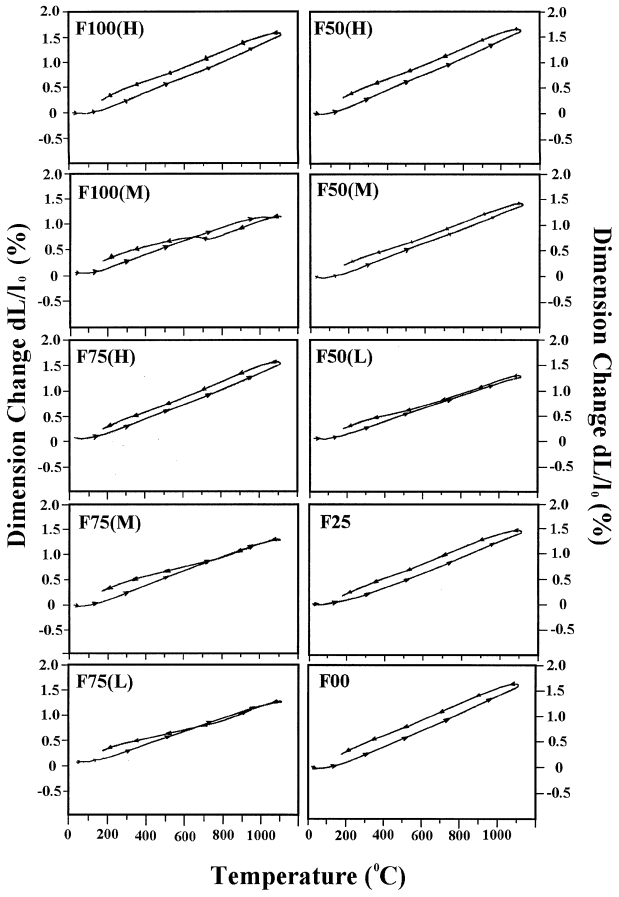

Fig. 3. Dilatometric and shrinkage curves of 10 PSZ plotted as a function of test temperature.

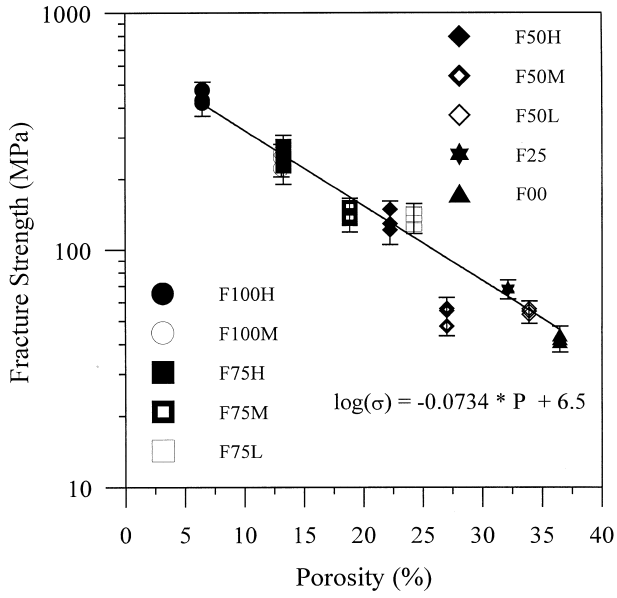

Fig. 4. Fracture strength tested at room temperature plotted as a function of the porosity of PSZ.

four specimens, including F100M, F75M, F75L and F50L, show their M_s temperatures as high as 650°C. Upon cooling, the linear contraction of four PSZ shows a t-to-m transformation. The phenomena are consistent for the PSZ samples with a higher fine-powder content (F100, F75 or F50) and sintered at 1450°C (Table 1). As long as the formulation contains more (>25%) coarse zirconia grains (stabilized AQZ powder) and densified at 1550°C or higher temperatures will be stabilized and not undergo t-to-m transformation.

3.3. Mechanical properties of PSZ at room temperature

The fracture strength at room temperature was measured and plotted as a function of porosity of PSZ (Fig. 4). The measured strength of the PSZ ranges from 441 to 52 MPa. The data can be fitted with an empirical equation which depicts the relationship of strength (σ) to porosity (p) below

$$\sigma = \sigma_0 \exp(-Cp) \quad (2)$$

where σ_0 is the strength of the samples without porosity (in %) and C is a constant. The values of σ_0 and C are 665 MPa and 0.073, respectively. The character of the fitting line reveals that the strength of the PSZ can be an exponential function of porosity, except for F50M (too low with respect to the fitting line). The possible strength of a fully dense PSZ is 665 MPa.

The SEM micrographs of three polished and HF acid-etched surfaces of the PSZ samples are shown in the right column of Fig. 5. Due to the abundance of porosity of these PSZ samples with the coarse grains of 50% or more, the grinding and polishing forces were greatly reduced to prevent grain pull-out. However, the grain pull-out was still occasionally found on the polished surfaces of F00 sample, resulting in a porosity over than that measured by Archimedes' method. The F100H sample [in Fig. 5(a)] has a uniform grain structure with the grain sizes of 20 to 50 μm and closed porosity in the sizes 4 to 16 μm. The t-phase grains revealed by etching have sizes less than 0.1 μm. As the matrix containing coarse grains, the microstructure of the sintered PSZ appears as fully dense regions corresponding to the coarse grains added in the formulation. The large grains are angular and mostly associated with tiny cracks as the F75L shown in Fig. 5(b). Connected pores (or cracks) as large as 160 μm were occasionally found associated with coarse ZrO_2. In comparison, F00 [Fig. 5(c)], which is an extreme case and made of 100% coarse powder, has 36% porosity. The grains of F00 are weakly bonded, and the pores in irregular shape are interconnected. The porosity in all samples is randomly distributed and in an irregular shape in the matrix.

The fracture surfaces of above mentioned PSZ samples are also shown in the left column of Fig. 5. The surfaces can be distinguished into three types, either a

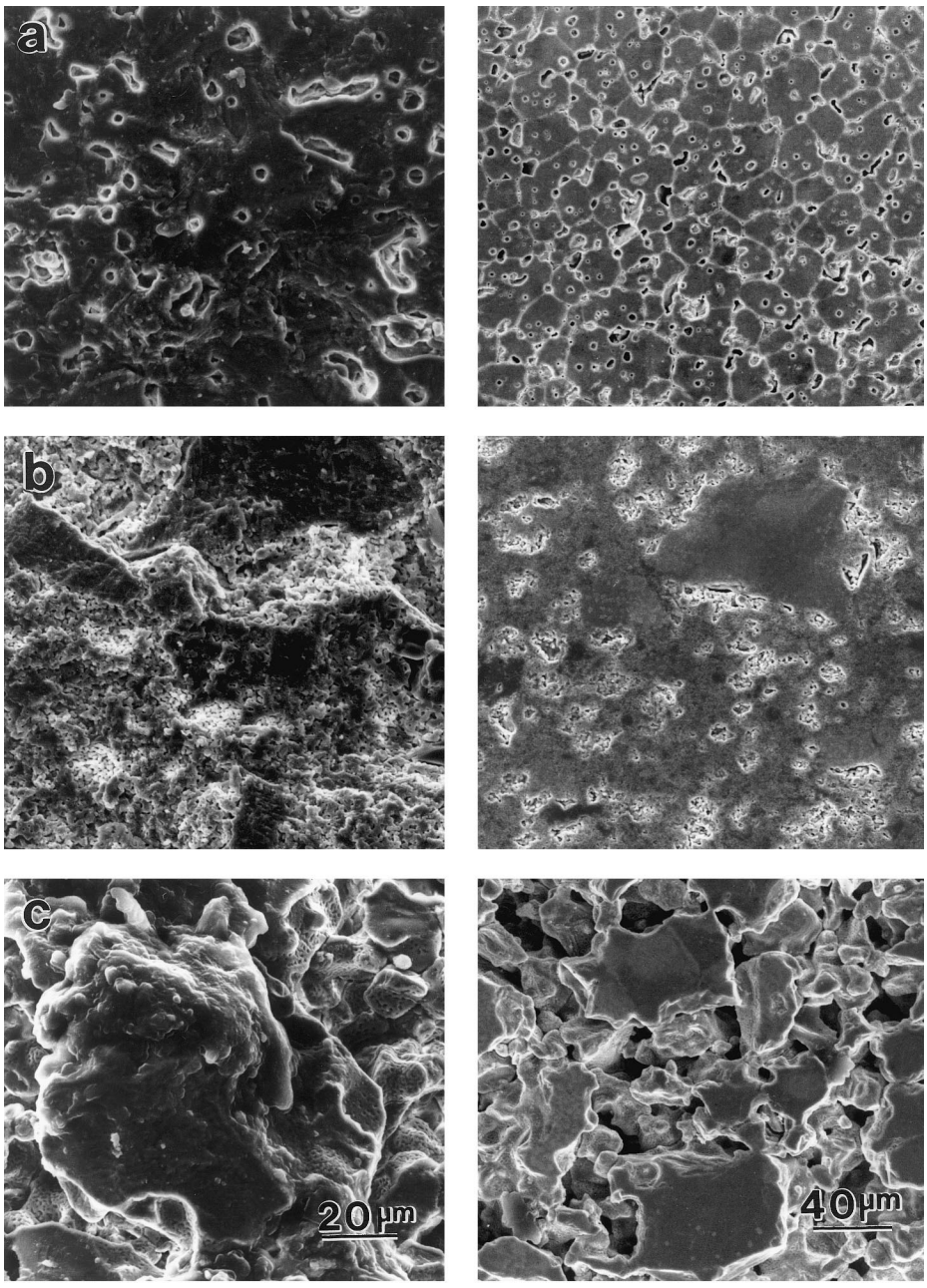

Fig. 5. SEM micrographs of the polished (right column) and fracture surfaces (left column) of the PSZ (a) F100H, (b) F75L, (c) F00 samples.

transgranular fracture, intergranular fracture, or a mixture. The transgranular fracture is dominate in two F100 and three F75 samples. The evidence observed is especially the fracturing of dense, large zirconia grains, as those in the micrographs of F100H and F75L in Figs. 5(a) and (b). The coarse grains in the first fracturing type depict a sharp surface[1], while the second types samples have the fracture surfaces having cracks passing along grain boundaries. Large grains with smooth surfaces in F25 or F00 specimens and no flat surface is observed [Fig. 5(c)].

Fig. 6 is the fracture toughness of 10 PSZ samples measured at room temperature. Four measurements of each sample are all plotted in the figure. The best toughness is the 5.4 MPa $m^{1/2}$ of F100H. In literature, the toughness of MgO–PSZ was reported ranging from 4.8[14] to 13.5 MPa $m^{1/2}$.[3] Some MgO–PSZ samples also have an *R*-curve behavior.[3] It is interesting to note that the data points in Fig. 6 cannot be formulated into one single curve, but rather separated into two curves in exponential function. Each behaves consistently with

[1] The surfaces of the coarse grains are mostly smooth, which is different from the grain surfaces exposed to sintering atmosphere [Fig. 5(c)]. Therefore, the flat regions in Fig. 5(b) are likely caused by the fracturing of coarse grain tested at room temperature.

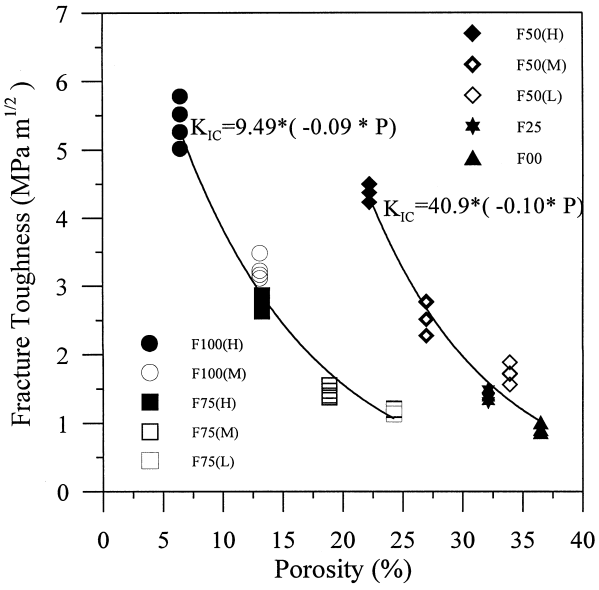

Fig. 6. Fracture toughness tested at room temperature plotted as a function of the porosity of PSZ. Note that the data are fitted into two curves.

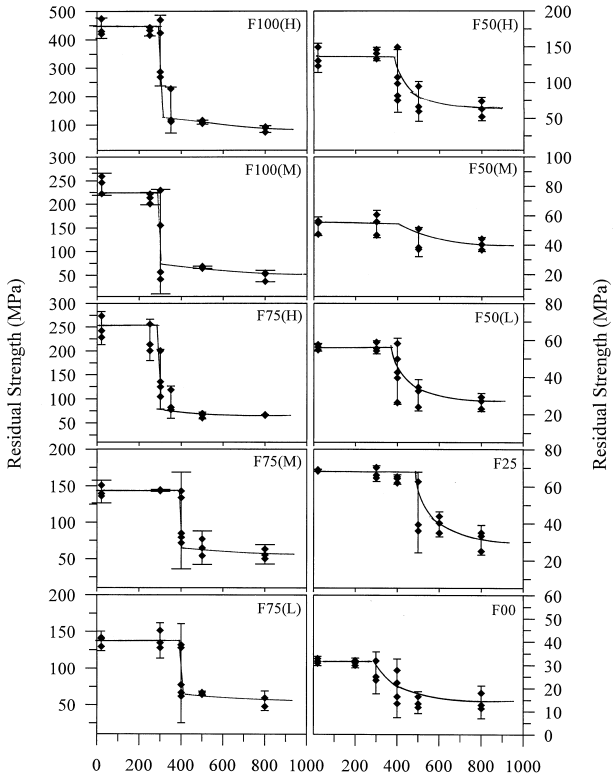

Fig. 7. Residual strength of PSZ plotted against critical quenching temperature difference (ΔT).

respect to their formulation. The content of coarse grains is distinguished in an amount of 50%, as shown in Fig. 6, implying that the factor(s) other than the porosity induced by the content of coarse grains should also control the fracture behavior of the PSZ.

3.4. Thermal shock resistance of PSZ

The residual strength (σ_r) of thermal shocked PSZ samples were measured and reported as a function of quenching temperature (ΔT), as shown in Fig. 7. The fitted curves in each sample reveal two fracturing behaviors. One appears to abruptly decrease in residual strength (type I) and the other decreases gradually (type II) when tested above a critical quenching temperature ΔT_c.

The type of fracture, the values of ΔT_c, the residual strength, and strength ratio (σ_r/σ_f), are recorded and shown in Table 2. The results in the table show that F25 has the highest value 500°C in ΔT_c. The F100H sample has the highest residual strength (85 MPa) and F50M has the greatest residual strength ratio (σ_r/σ_f) of 77% among all PSZ, as shown in Fig. 7.

The fracture energy (γ_f) of each PSZ was calculated according to the Griffith equation:

$$\gamma_f = \frac{K_{IC}^2(1-\nu^2)}{2E} \quad (3)$$

where γ_f is obtained from the values of E, K_{IC} and ν, shown in the last column of Table 1. The calculated fracture energy has the values from 4.6 to 64.2 J/m^2 which is far less than the report (ca. 290 J/m^2) of the Mg–PSZ[15] annealed at 1000°C.

4. Discussion

Several parameters of thermal shock resistance for the evaluation of ceramic materials have been proposed and reviewed in literature.[16–19] A parameter, R, corresponds to the critical temperature, ΔT_c, which is thought to be the point that the thermal stress on the surface of a test piece equals to the fracture strength. In addition, R‴, R⁗ and the others are also used. These were considered in a relatively scale to reveal the resistance to the initiation or propagation of cracks, and to rank the relative capability of the thermal shock resistance of materials. The parameters are formulated as a combination of material properties, for instance Young's modulus, coefficient of thermal expansion (CTE), Poisson's ratio, and fracture strength.

Hasselman[17,18] pointed out that pre-existing cracks and normalized quench temperature, $\Delta T/\Delta T_c$, strongly influence crack growth behavior and residual strength after thermal shock. A ceramic material containing shorter cracks, L_0, less than a characteristic length, L_f, shows a drastic drop in strength when the quench temperature ΔT is greater than ΔT_c. The released elastic

Table 2
Fracture mode, critical quenching temperature difference, residual strength ratio, largest tolerable crack size and four thermal shock parameters of the PSZ samples[a]

	Fracture mode	ΔT_c (°C)	σ_r (MPa)	σ_r/σ_0 (%)	a_t (μm)	R (K)	R''' ($\times 10^{-16}$/Pa)	R'''' (m)	R_{st} (K m$^{1/2}$)
F100H	Type I	300	85	19	38	113	4.4	70.3	1.27
F100M	Type I	300	52	21	45	96	5.4	87.1	1.05
F75H	Type I	300	66	27	30	74	3.5	57.6	0.69
F75M	Type I	400	56	39	26	56	6.0	69.2	0.63
F75L	Type I	400	56	41	19	74	6.2	61.4	0.73
F50H	Type II	400	63	47	278	47	40.4	527	1.34
F50M	Type II	400	41	77	601	26	108	1142	1.10
F50L	Type II	400	25	46	106	42	70	199	0.89
F25	Type II	500	31	46	252	49	30.5	475	1.16
F00	Type II	300	15	36	121	27	32.2	229	0.51

[a] Where $R = \sigma_f(1-\nu)/E\alpha$, $R''' = \gamma/\sigma_f^2(1-\nu)$, $R'''' = \gamma E/\sigma_f^2$, and $R_{st} = \left(\gamma/\alpha^2 E\right)^{1/2}$.

energy is adsorbed due to the extension of catastrophic cracks. But for the material with longer cracks, $L_0 > L_f$, the strength decreases gradually while testing under $\Delta T > \Delta T_c$, implying that the cracks would propagate in a quasi-static manner. Two fracture modes of the retaining strength after thermal shock are categorized as type I or II, respectively.

4.1. Porosity and characteristic defect length

The ratio of the fine/coarse powder in PSZ formulation influences the sintering results in several aspects. The amount of the porosity and the pore dimension decreases as the content of the fine powder increases. As consequence, the material properties, including Young's modulus, shear modulus, especially the fracture strength and toughness, change accordingly as the state of the porosity varies.

The densest sample [F100H in Fig. 5(a)] has a uniform grain structure with closed pores in the sizes less than 15 mm located at the grain boundaries. No microcracks is found, except some fine precipitates of magnesium zirconate found at grain boundaries, identified by TEM and EDS.[20,21] The t-phase precipitates revealed by etching have the sizes of 0.1 μm and is smaller than that of the pores at grain boundaries.

The pores are the most predominant defects in the PSZ. Large zirconia grains are angular in sintered matrix and mostly surrounded with continuous pores, e.g. F75L in Fig. 5(b). These porous channels can be treated as the nucleation site of cracks and are frequently observed in the PSZ contained coarse grains. The size distribution of the pores is difficult to quantify from the ceramographic pictures. As a result, the defect size is hard to quantify too.

For simplification of the states of pores (defects), the greatest length (a_t) of defect is introduced. It represents a characteristic length of a nominal largest defect of which the PSZ can stand without catastrophic failure. The a_t value can be determined from the toughness and strength of brittle PSZ specimens by Griffith relationship. Then, the a_t is

$$a_t = \frac{1}{\pi}\left(\frac{K_{IC}}{1.12\sigma_f}\right)^2 \tag{4}$$

if the defect size is much smaller than the dimension (W) of the test piece, i.e. a small a_t/W.[22] The calculated a_t values of each PSZ are shown in the sixth column of Table 2. It is noted that the PSZ with type II fracture mode has the tolerable defect length in the range of 106 to 601 μm, which is ca. 10 times higher than those of type I samples. The largest value (600 μm) of a_t is shown for the F50M sample which has 50% coarse grains in the formulation and shows 27% porosity. It is the optimized condition that the test piece has the best tolerance to the testing condition. The residual strength (σ_r/σ_f) of F50M is the best among 10 PSZ samples.

The state of the defects would change, for instance the crack length increases during thermal shocking. The criteria of the crack extension either in Type I or II are controlled by the original crack length relative to characteristic length (l_f) and testing condition ΔT.[17] Knudsen reported[23] that the fracture strength of ceramics is sensitive to structural defects and is controlled not only by grain size, also by the dimensions of pre-existing cracks. The porosity, a matter of important fracture origins, decreases the strength of the material.

The MgO–PSZ prepared in this study has the toughness ranging from 0.9 to 5.4 MPa m$^{1/2}$. The reported R-curve behavior,[3] which means the PSZ would increase in resistance to crack propagation as the length of the crack extends, is not observed in our PSZ samples. The toughness[4] is strongly dependent on the size and the amount of the t-phase precipitate in PSZ. The transformation toughening seems not operate in the cases. The variation of toughness and fracture strength is controlled by the pre-existing defects (pores and cracks) of

the PSZ, and in fact by the coarse/fine powder ratio in the formulation. But, these mechanical properties are not directly correlating to the thermal shocking behavior. The PSZ shows two groups of thermal shock resistance in Table 2. Type I with a denser matrix, and Type II with a high value of ΔT, σ_r/σ_0, and a_t. The later (e.g. F50M and F25) is not necessarily performing a high toughness.

4.2. Thermal shock resistance

The following thermal shock parameters, R, R‴, R⁗ and R_{st} are calculated according to the mechanical and material properties shown in Table 1[17,18]

$$R = \sigma_f(1-v)/E\alpha \quad (5)$$

$$R''' = \gamma/\sigma_f^2(1-v) \quad (6)$$

$$R'''' = \gamma E/\sigma_f^2 \quad (7)$$

and

$$R_{st} = (\gamma/\alpha^2 E)^{1/2} \quad (8)$$

As depicted in Table 2, a highest R value (113 K) is performed on F100H, the highest R''' and R'''' (108×10^{-16}/Pa and 1142 m, respectively) are achieved by F50M, and a best ΔT_c (500°C) is noted on F25. These PSZ samples behaved very differently.

The best resistance to strength degradation (σ_r/σ_0) in the PSZ samples is F50M which performs a type II fracture. Four properties, ΔT_c (400°C), R''', R'''' and σ_r/σ_0 (76%) of F50M are nearly the best among all PSZ samples. For the samples with a type II fracture, the best ΔT_c is 500°C (F25). The F25 sample in fact has the highest R value (49 K). For the samples with type I fracture, the F100H has the greatest R value and the highest residual strength (85 MPa) among the tested PSZ, but its ΔT_c is 300°C only.

It is difficult to address the relationship between thermal shock parameters with ΔT_c and σ_r/σ_0 without concerning the types of fracture. The samples with type I fracture mode have lower ΔT_c, σ_r/σ_0 and a_t which do not appear to have any relationship with R and R_{st} as the parameters shown in Table 2. However, the residual strength ratio (σ_r/σ_0), R''' and R'''' having a relationship can be shown as Fig. 8(a). The higher the R''' and R'''', the better the σ_r/σ_0. PSZ samples with a porous character perform type II fracture and have a better thermal shock properties in R''' and R''''. The results appear that the σ_r/σ_0 values are in general greater than 40% and better than the samples with type I fracture.

Fig. 8(b) depicts the dependence of two shock resistant parameters on the greatest length a_t of defect. A characteristic length of defects, L_f, is noted which

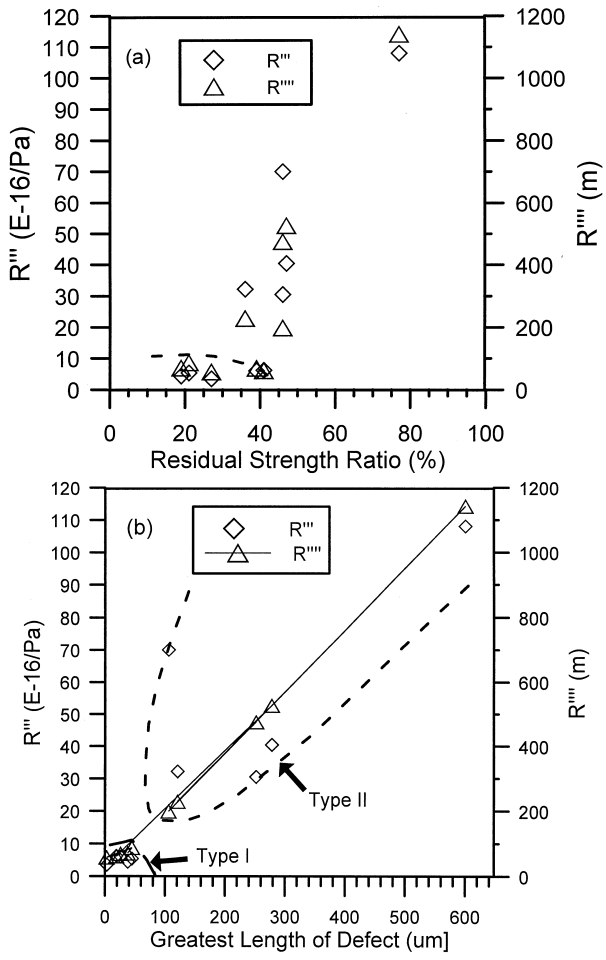

Fig. 8. Thermal shock parameters, R''' and R'''', plotted against (a) residual strength ratio and (b) greatest length of defect a_t.

separates the samples to two groups with the boundary in Fig. 8(b). The value of L_f is in the size ca. 80 μm. The samples with either type I or II thermal shocking behavior can be distinguished by the boundary, the position of the characteristic length L_f of defect. That implies if the PSZ contains a defect in a size L_0 less than the characteristic length, 80 μm, the matrix undergoes a drastic drop in strength when the quench temperature is greater than ΔT_c. Type I shocking fracture takes place. But for the material with greater defects with a size longer than 80 μm, the strength decreases gradually when testing at ΔT higher than ΔT_c. The defects (pores) might extend in a quasi-static condition and result in greater residual strength ratio and ΔT_c.

5. Conclusion

The fraction of fine powder in the mixture is important for the sintering and thermal shock properties of PSZ materials. The properties of 10 Mg–PSZ with various microstructures and identical t/m phase ratios were evaluated, and revealed the following.

1. Young's modulus and shear modulus are not a function of the ratio of fine/coarse addition, but a relationship with the porosity of sintered PSZ. The highest values are 213 GPa (E) and 142 GPa (G) (F100H), respectively. The Poisson's ratio and linear thermal expansion coefficient of made PSZ are 0.2 ± 0.05 and $12.8 \pm 1.2 \times 10^{-6}$/K, respectively, independent upon the porosity and the amount of fine powder.
2. The highest fracture strength is 441 MPa of F100 (sintered at 1700°C for 4 h) among all PSZ samples. The strength of the PSZ is an exponential function to the porosity of sintered PSZ.
3. There are two fracture mechanisms operating in the thermal shocked PSZ. Transgranular fracture occurs in the specimens with a fraction of fine powder more than 0.5. The highest fracture toughness value is $5.4\ \mathrm{MPa}\sqrt{\mathrm{m}}$ (F100H); The other is intergranular fracture for the specimens with a fraction of fine powder less than 0.5. The resulting fracture toughness has the highest value, $4.4\ \mathrm{MPa}\sqrt{\mathrm{m}}$ (F50H). In each group, the fracture toughness decreases with an increase in porosity.
4. Three PSZs perform the best in thermal shock resistance. F50M has $\Delta T_c = 400°C$, $R''' = 108$, and a residual strength ratio of 77%. F100H has a best R value (113 K) and a greatest residual strength (85 MPa) among the tested specimens. The highest ΔT_c is 500°C (F25) which has the highest R value among the samples with type II fracture.
5. Strong correlation between the largest tolerable defect size a_t to two thermal shock properties, R''' and R''''. The samples perform either type I or type II thermal shock behavior which can be differentiated by a characteristic length L_f of defect. The value of the L_f is determined in a size ca. 80 μm.

Acknowledgements

The authors gratefully acknowledge the support of the National Science Council (NSC86-2216-E-002-020) and Tjing Ling Industrial Research Institute (86-G-14) at the National Taiwan University.

References

1. Kienow, S., Refractory materials, *Interceram*., 1979, **28**(3), 1–18 (Ceramic Monograph).
2. Bullard, R. L. and Cheng, P. C., Long term casting with zirconia nozzles. *Iron & Steelmaking*, 1992, June, 19–26.
3. Heuer, A. H., Transformation toughening in ZrO_2-containing ceramics. *J. Am. Ceram. Soc*., 1987, **70**(10), 689–698.
4. Green, D. J., Hannink, R. H. J. and Swain, M. V. *Transformation Toughening of Ceramics*. CRC Press, Inc., 1989.
5. Ramaswamy, P., Narayana, B. H. and Vynatheya, S., Thermomechanical and microstructural evaluation of high tmeperature sintered (Mg, Mg–Ti)-PSZ. *Ceram. Int*., 1996, **22**, 287–293.
6. Hannink, R. H. J. and Garvie, R. C., Subeutectoid aged Mg–PSZ alloy with enhanced thermal up-shock reistance. *J. Mat. Sci*., 1982, **17**, 2637.
7. Lutz, H. E., Swain, V. M. and Claussen, N., Thermal shock behavior of duplex ceramics. *J. Am. Ceram. Soc*., 1991, **74**(1), 19–24.
8. Cotterell, B., Ong, S. W. and Qin, C., Thermal shock and size effects in castable refractories. *J. Am. Ceram. Soc*., 1995, **78**(8), 2056–2064.
9. Schon, S., Prielipp, H., Janssen, R., Rodel, J. and Claussen, N., Effect of microstructural scale on thermal shock resistance of aluminum-reinforced alumina. *J. Am. Ceram. Soc*., 1994, **77**(3), 701–704.
10. Wei, W. and Lin, Y. P., Processing character of MgO–partial stabilized zirconia (PSZ) in size grading prepared by injection molding. *J. Eur. Ceram. Soc*., 1998, **18**, 2107–2116.
11. Garvie, R. and Nicholson, P. S., Phase analysis in zirconia systems. *J. Am. Ceram. Soc*., 1972, **55**(6), 303–305.
12. Wang, J., Rainforth, W. M., Wadsworth, I. and Stevens, R., The effects of notch width on the SENB toughness for oxide ceramics. *J. Eur. Ceram. Soc*., 1992, **10**, 21–31.
13. Morrell, R., *Handbook of Properties of Technical & Engineering Ceramics, Part 1, An Introduction for the Engineer and Designer*. National Physical Laboratory, London, 1985.
14. Nettleship, I. and Stevens, R., The effect of cooling rate on the phase transformations in Mg–PSZ. *Br. Ceram, Trans, J*., 1987, **86**(6), 183–186.
15. Hughan, R. R. and Hannink, R. H. J., Precipitation during controlled cooling of magnesia–partially-stabilized zirconia. *J. Am. Ceram. Soc*., 1986, **69**(7), 556–563.
16. Hasselman, D. P. H., Elastic energy at fracture and surface energy as design criteria for thermal shock. *J. Am. Ceram. Soc*., 1963, **46**(11), 535–540.
17. Hasselman, D. P. H., In *Ceramics in Severe Environments*, ed. Kriegel and Palmour III. Plenum Press, New York, 1971, pp. 89–103.
18. Hasselman, P. D. H., Figures-of-merit for the thermal stress resistance of high-temperature brittle materials: a review. *Ceramurgia Int*., 1978, **4**(4), 147–150.
19. Arnold, M., Boccaccini, A. R. and Ondracek, G., Theoretical and experimental considerations on the thermal shock resistance of sintered glasses and ceramics using modelled microstructure–property correlations. *J. Mat. Sci*., 1996, **31**, 463–469.
20. Lin, Y. P., Master thesis, National Taiwan University, May 1997.
21. Farmer, S. C., Schoenlein, L. H. and Heuer, A. H., Precipitation of $Mg_2Zr_5O_{12}$ in MgO–partial stabilized ZrO_2, *Comm. Am. Ceram. Soc*., 1985, July, C107–109.
22. Broek, D., *Elemental Eng. Fract. Mechanics*, 1984.
23. Knudsen, F. P., Dependence of mechanical strength of brittle polycrystalline specimens on porosity and grain size. *J. Am. Ceram. Soc*., 1959, **42**, 376.